



## Mobile atmospheric measurements and local-scale inverse estimation of the location and rates of brief CH<sub>4</sub> and CO<sub>2</sub> releases from point sources

Pramod Kumar<sup>1</sup>, Grégoire Broquet<sup>1</sup>, Camille Yver-Kwok<sup>1</sup>, Olivier Laurent<sup>1</sup>, Susan Gichuki<sup>1</sup>,  
Christopher Caldwell<sup>1</sup>, Ford Cropley<sup>1</sup>, Thomas Lauvaux<sup>1</sup>, Michel Ramonet<sup>1</sup>, Guillaume Berthe<sup>2</sup>,  
5 Frédéric Martin<sup>2</sup>, Olivier Duclaux<sup>3</sup>, Catherine Juery<sup>3</sup>, Caroline Bouchet<sup>4</sup>, Philippe Ciais<sup>1</sup>

<sup>1</sup>Laboratoire des Sciences du Climat et de l'Environnement (LSCE/IPSL), CEA-CNRS-UVSQ, 91191 Gif-sur-Yvette, France

<sup>2</sup>IFP Energies nouvelles-Géoscience, 92852 Rueil-Malmaison Cedex, France

<sup>3</sup>TOTAL Laboratoire Qualité de l'Air (LQA), 69360 Solaize Cedex, France

<sup>4</sup>SUEZ-Smart & Environmental Solutions, Tour CB21/16 place de l'Iris, 92040, La Défense, France

10 *Correspondence to:* Pramod Kumar (pramod.kumar@lscce.ipsl.fr)

### Abstract

We present a local-scale atmospheric inversion framework to estimate the location and rate of methane (CH<sub>4</sub>) and carbon dioxide (CO<sub>2</sub>) releases from point sources. It relies on mobile near-ground atmospheric CH<sub>4</sub> and CO<sub>2</sub> mole fraction measurements across the corresponding atmospheric plumes downwind the  
15 sources, on high-frequency meteorological measurements, and a Gaussian plume dispersion model. It exploits the spread of the positions of individual plume cross-sections and the integrals of the gas mole fractions above the background within these plume cross-sections to infer the position and rate of the releases. It has been developed and applied to provide estimates of brief controlled CH<sub>4</sub> and CO<sub>2</sub> point source releases during a one-week campaign in October 2018 at the TOTAL's experimental platform  
20 TADI in Lacq, France. These releases lasted typically 4 to 8 minutes and covered a wide range of rates (0.3 to 200 gCH<sub>4</sub>/s and 0.2 to 150 gCO<sub>2</sub>/s) to test the capability of atmospheric monitoring systems to react fast to emergency situations in industrial facilities. It also allowed testing their capability to provide precise emission estimates for the application of climate change mitigation strategies. However, the low and highly varying wind conditions during the releases added difficulties to the challenge of  
25 characterizing the atmospheric transport over the very short duration of the releases. We present our series of measurements of CH<sub>4</sub> and CO<sub>2</sub> mole fractions using instruments onboard a car that drives along the roads ~50 to 150 m downwind the 40 m × 60 m area of controlled releases for each of the releases and the results from the inversions of the release locations and rates. The comparisons of these results to the actual position and rate of the controlled release indicate a 20%-30% average error on the release rates  
30 and a ~30-40m errors in the estimates of the release locations. These results are shown to be promising especially since better results could be expected for longer releases and under meteorological conditions more favorable to local scale dispersion modeling.



## 1. Introduction

35 Accurate detection and quantification of greenhouse gas (GHG) emissions from anthropogenic activities  
is essential to construct effective mitigation policies. A large fraction of pollutant and greenhouse gases  
comes from industrial sites. Between 30% and 42% of the anthropogenic emissions of methane (CH<sub>4</sub>)  
between 2008 and 2017 are from the fossil fuel production and use sector (coal, natural gas and oil)  
according to Saunio et al. (2019). A recent study by Hmiel et al. (2020) suggests that anthropogenic  
40 fossil CH<sub>4</sub> emissions have been underestimated by about 38 to 58 Tg/year, which could implicitly rise the  
contribution of this sector by 25%-40%. CH<sub>4</sub> emissions estimates for specific sectors by inventories  
combine uncertain activity data and highly uncertain emission factors (Alvarez et al., 2018). Furthermore,  
typical emission factors used as default values in inventories can hardly be representative of the specific  
configurations and processes of individual sites, and, in practice they are usually different from those  
45 measured at specific sites (e.g. Vaughn et al., 2017; Ravikumar et al., 2017; Omara et al., 2018)  
Monitoring of CH<sub>4</sub> emissions from individual sites and even at the scale of local facilities within the same  
site is thus recommended to assess the effectiveness of local measures applied to minimize emissions  
(Konschnik et al., 2018).

CH<sub>4</sub> emissions from industrial activities are often strongly localized and can occur at many places with  
50 all kinds of frequency or temporal scales (continuous to infrequent, constant, highly variable) (Zavala-  
Araiza et al., 2018). CH<sub>4</sub> can be emitted at various stages of activities related to oil and gas production,  
transport, and use, e.g., venting during oil extraction, pressure controllers, unintended fugitive emissions  
across the entire process chain, pressure regulators along distribution through pipelines, and storage  
(Höglund-Isaksson, 2017). Some of these emissions could be localized and quantified through periodical  
55 LDAR (Leak Detection and Repair) campaigns. Some others are more difficult, as they do not relate to  
easily measurable processes. Such CH<sub>4</sub> emissions are often accompanied by CO<sub>2</sub> emissions, e.g. when  
considering diesel engines powering large compressors or flaring activities to reduce natural gas (NG)  
venting (Caulton et al. 2014). Therefore, the monitoring of CO<sub>2</sub> emissions whose budget can be significant  
and which can help detect and characterize the processes underlying the CH<sub>4</sub> emissions is important too.

60 For Oil and Gas (O&G) related activities, fugitive emissions e.g. from leaky valves or air bleeds from  
compressors should be distinguished from intermittent emissions that occur during nominal and  
maintenance operations e.g. purging and draining of pipes. Several recent studies have shown that a few  
leaks, often referred to as super-emitters, can be responsible for a large fraction of O&G emissions of a  
site, creating a long-tail distribution of emission sources (Omara et al., 2016; Zavala-Araiza et al.,  
65 2015, 2017; Frankenberg et al., 2016; Alvarez et al., 2018). Therefore, reducing infrequent but large  
releases of CH<sub>4</sub> is an effective strategy for reducing the overall emissions of the entire O&G sector (Duren  
et al, 2019). In addition to their effect on climate, large sporadic CH<sub>4</sub> emissions can also be an issue for  
safety, a further argument for having systems to allow their fast detection and quantification.



70 Atmospheric CH<sub>4</sub> and CO<sub>2</sub> concentration measurements in the vicinity of industrial sites, or of facilities  
within a site have been used for detecting, localizing and quantifying local emissions. These data are  
combined with tracers or transport models for the localization of the sources, and dual tracer methods,  
mass balance approaches or atmospheric transport inverse modelling techniques to quantify their release  
rates (Foster-Wittig et al., 2015; Albertson et al., 2016; Ars et al., 2017; Yacovitch et al., 2017; Feitz et  
al., 2018; etc.). Current measurement methods include both in situ and remote sensing measurements  
75 from fixed stations or mobile platforms (with instruments onboard aircraft, automobile, or drones)  
(Peischl et al., 2013; Pétron et al., 2014; Brantley et al., 2014; Goetz et al., 2015; Foster-Wittig et al.,  
2015; Albertson et al., 2016; Alvarez et al., 2018; Feitz et al., 2018; Cartwright et al., 2019, etc.). In order  
to develop, test and improve atmospheric measurement and modeling techniques to detect, localize and  
quantify emissions, controlled release experiments have been regularly conducted (Loh et al., 2009;  
80 Lewicki and Hilley, 2009; Ro et al., 2011; Humphries et al., 2012; Kuske et al., 2013; van Leeuwin et al.,  
2013; Luhar et al., 2014; Foster-Wittig et al., 2015; Jenkins et al., 2016; Hirst et al., 2017; Ars et al., 2017;  
etc.).

TOTAL developed the so-called TOTAL Anomaly Detection Initiatives (TADI) platform at Lacq in  
southwestern France as a test bed of different GHG measurement technologies and emission detection  
85 and quantification methods that could be implemented to support either the fast detection of large leaks  
or for the estimate of the long-term budget of the GHG emissions from facilities. On this TADI platform  
there could be reproduced around 30 different leaks scenarios among the most common ones potentially  
occurring on operational sites (cold venting, leaks from a flange, leaks from a connection, leakage of  
valves, leakage under insulation, corrosion on a line, etc.) thanks to the diversity of industrial equipment  
90 implemented (pipes, valves, tanks, columns, wellhead, flare, etc.). In October 2018, a one-week campaign  
was held at the TADI platform to evaluate different approaches for determining the precise location and  
magnitude of brief CH<sub>4</sub> and CO<sub>2</sub> controlled releases from point sources. Different groups with various  
atmospheric measurement and modelling techniques participated in the campaign. With typically 4-8-  
minute releases, the experiment was mainly designed for testing safety surveillance systems addressing  
95 emergency situations rather than for testing the ability to quantify routine emissions accurately on the  
long run. However, a wide range of rates were used for the controlled releases, including large ones that  
can raise safety issues but also small ones, which mainly raise concerns for climate change. Such a wide  
range of sporadic releases was a challenge for the systems deployed by the participants since requiring a  
good instrumental precision for both low and high signals in the atmospheric concentrations, and the  
100 analysis of atmospheric processes over short durations.

We participated in this campaign within the framework of the TRACKing Carbon Emissions (TRACE)  
program (<https://trace.lsce.ipsl.fr/>), using a mobile measurement strategy similar to that of Yver Kwok et  
al. (2015) and Ars et al. (2017), with a CRDS instrument onboard of a vehicle driven back and forth  
across CH<sub>4</sub> and CO<sub>2</sub> plumes to take as many cross-sections as possible of each release. The measurements



105 were made along roads downwind the TADI platform with the air intake located ~2 m above the ground.  
Currently, such mobile measurements cannot be conducted continuously, so that they are hardly adapted  
to a continuous screening for fast detection of dangerous leaks. However, such measurements could be  
conducted regularly to get a representative diagnostic of emissions from a site and of their evolution with  
time. Furthermore, the development of automated mobile platform with light instruments could allow for  
110 the use of such a measurement strategy for a more systematic monitoring of the emissions from a site.

One traditional way of quantifying emissions from a source with concentration measurements along  
plume line cross-sections near the ground is to release a tracer with a known rate close to this targeted  
source and to exploit the concentration ratios between the targeted gas and the tracer (Yver Kwok et al.,  
2015). However, one can hardly conduct such tracer releases for regular campaigns or continuous  
115 monitoring, or within areas exposed to safety issues. Furthermore, the method hardly helps localizing the  
targeted source. It actually relies on a good knowledge of its position. The use of dispersion models to  
analyze such data for the estimate of source locations and rates can be challenging (Foster-Wittig et al.,  
2015; Ars et al. 2017). Furthermore, most of the atmospheric inversion approaches to localize and  
quantify point sources have been developed and tested for releases lasting ~30 min or more (Feitz et al.,  
120 2018) whereas the TADI releases during this campaign did not exceed 18 minutes. Because of the short  
duration of those releases, only a small number of plume cross-sections could be obtained for each of  
them, limiting the robustness of the inversions. Finally, the meteorological conditions during the  
campaign were quite challenging, with low wind speed and highly varying wind directions. We had to  
develop a specific and pragmatic inversion approach to overcome these challenges, exploiting the spread  
125 of the positions of the few individual plume crossing and the integrals of the concentration above the  
background within these plume crossings to infer the position and rate of the brief releases. It is based on  
a Gaussian plume model whose parameters were fixed using the meteorological measurements conducted  
on the TADI platform. Its successful retrieval of relatively good release location and rates confirm that it  
could feed more advanced strategies for the local scale monitoring of GHG emissions.

130 This study documents our measurements, analysis, inversions and the comparison of the results to actual  
release location and rates during the TADI-2018 campaign. In section 2, we detail the experimental setup  
and atmospheric measurements. The theoretical and computational frameworks of the inversion approach  
are described in section 3. Section 4 details the data analysis for the configuration of the transport model  
and inversion. The results and perspective of the study are discussed respectively in sections 5 and 6,  
135 followed by the conclusions in section 7.



## 2. The TADI-2018 campaign

### 2.1 The site, controlled releases and atmospheric conditions

The TADI-2018 campaign was conducted during October 15-19, 2018 at TOTAL's TADI platform in Lacq, northwest of Pau. The platform is a rectangular area of approximately 20000 m<sup>2</sup> with decommissioned oil and gas equipment installed to mimic typical equipment of a "real-world" oil and gas facility. Within the platform, there are different points from which CH<sub>4</sub> and / or CO<sub>2</sub> can be released at controlled rates from low to relatively high. There are chemical and industrial plants on the field East of the platform, and the surrounding area has agricultural land and rural settlements. The terrain of the TADI platform is almost flat. However, during controlled release experiments, tents for installing the instruments, the decommissioned oil and gas equipment, and other small infrastructure for storage create obstacles to dispersion and increase the roughness and inhomogeneity of the TADI platform. Figure 1 shows a schematic of our experimental setup during the TADI-2018 campaign.

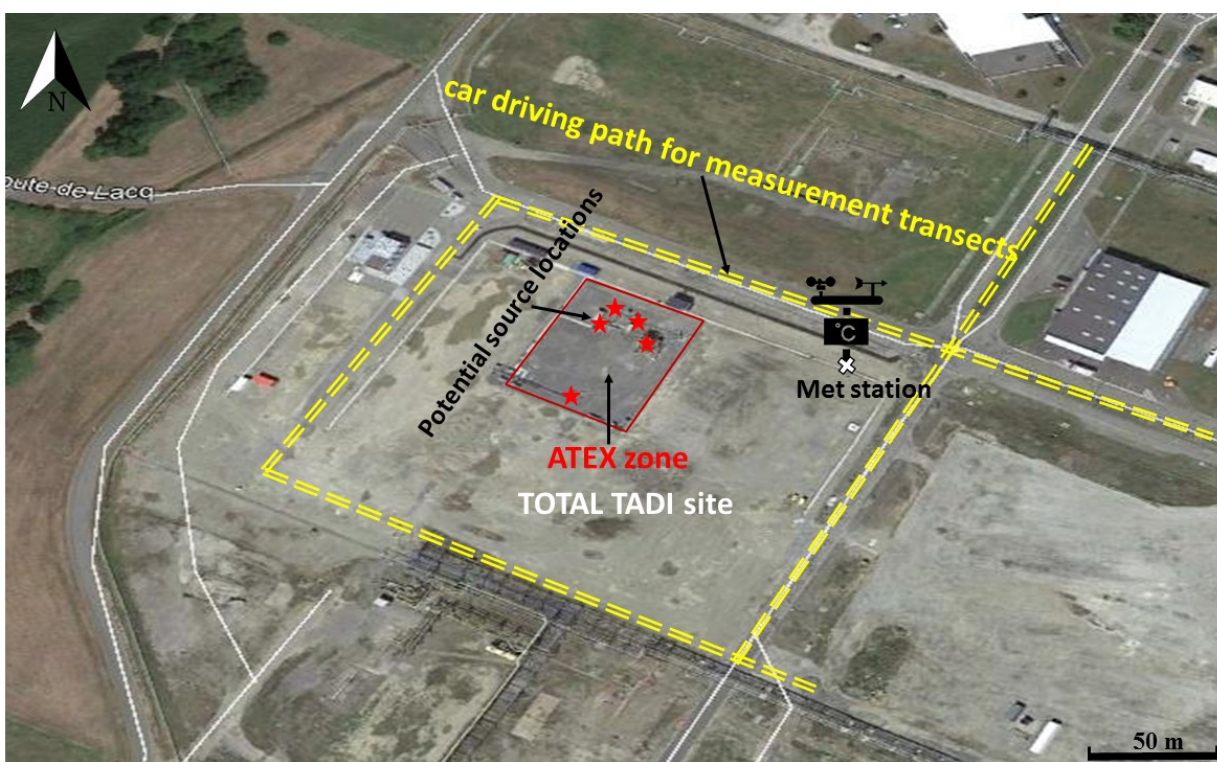


Figure 1: A schematic of the experimental setup on the top of the satellite image of the TADI platform (source: Google Earth). The red stars show the possible location of the emission sources in the ATEX zone (rectangle with red colored line). A hybrid SUV drove in electric mode on the road next to the site as shown by yellow colored double dotted lines. The meteorological station installed and operated by TOTAL was located at the basis of its black symbol.



155

During the campaign, a total of 50 CH<sub>4</sub> and CO<sub>2</sub> releases were carried out. All these controlled releases were made from different point source locations within a 40 m × 60 m rectangular area classified as the “ATEX zone” (Fig. 1), which for security reasons was cordoned off and out of reach for all participants. These point sources correspond to various type of equipment and release scenarios: drilled plugs, pipes, rack corrosion, flanges, valves, control boxes, horizontal or vertical tubing, horizontal or vertical piping, manhole, under insulation, tanks, scrubbers, product skids (red stars in Fig. 1) with different release heights between 0.1m to 6.5m above the ground. Mass flow controllers were used to control the releases of CH<sub>4</sub> and CO<sub>2</sub>. Several series of releases were performed with pauses of approximately 5 minutes between two releases and with a range of emission rates varying from 0.3 g/s to 200 g/s for CH<sub>4</sub> and from 0.2 g/s to 150 g/s for CO<sub>2</sub>. This setup allowed the reproduction of a variety of gas release scenarios expected in an industrial environment.

## 2.2 Atmospheric measurements

Atmospheric CH<sub>4</sub> and CO<sub>2</sub> measurements were obtained using two Picarro Cavity Ring Down Spectrometers (CRDS) with Picarro G2203 and G2401 analyzers for CH<sub>4</sub> and CO<sub>2</sub>, respectively. The analyzers were calibrated at the beginning and end of the experiment using high and low range calibration standards traceable to the WMO scales (WMOX2007 for CO<sub>2</sub>, and WMOX2004A for CH<sub>4</sub>; WMO GAW report No. 242; Table 1). Each standard was measured for at least 20 minutes on each analyzer. The agreement errors between the analyzer raw data and the calibration standard were smaller than 0.7% in CO<sub>2</sub> and 0.2% in CH<sub>4</sub>. Yver Kwok et al. (2015) had shown that within the mole fraction range of the WMO scales the analyzer precision of a range of CRDS analyzers including the G2401, defined as the raw data standard deviation over one minute, was <0.05 ppm and <0.5 ppb for CO<sub>2</sub> and CH<sub>4</sub>, respectively. The G2203 analyzer is based on identical spectroscopy as the CRDS analyzers investigated in this study. It was tested in a similar way during S. Ars PhD study and displayed similar performance (Ars, 2017). CRDS instruments are known to be stable within <0.15 ppm per year for CO<sub>2</sub> and <2.2 ppb per year for CH<sub>4</sub> (Yver Kwok et al., 2015).

Table 1: Assigned mole fraction of calibration standards used during the campaign, SD refers to the calibration reproducibility, which is defined as the standard deviation ( $1\sigma$ ) of the means of at least 3 independent measurements.

	CO <sub>2</sub> (ppm)	CO <sub>2</sub> SD (ppm)	CH <sub>4</sub> (ppb)	CH <sub>4</sub> SD (ppb)
High	522.25	±0.01	6135.03	±0.23
Low	411.94	±0.01	1980.65	±0.11



185 During the campaign the range of measured mole fractions corresponding to the releases selected for the  
inversions (see section 4.2) was 1.9 – 84 ppm for CH<sub>4</sub> and 400 – 800 ppm for CO<sub>2</sub>, with less than 4% of  
CH<sub>4</sub> and less than 2% of CO<sub>2</sub> measurements being higher than the CRDS calibration range shown in  
Table 1. The manufacturer specifications recommend operating ranges of 0-20 ppm CH<sub>4</sub> and 0-1000 ppm  
CO<sub>2</sub> for the G2203 and G2401 analyzers, respectively. In practice the analyzers were still operational  
190 over a higher range although lower performance may be expected in this case. To investigate the  
performance of both analyzers at high mole fractions, a linearity test was conducted at the Laboratoire  
des Sciences du Climat et de l'Environnement (LSCE) over a mole fraction range of 2 - 50 ppm CH<sub>4</sub> and  
400 - 5000 ppm CO<sub>2</sub>, which spans ~99% of the CH<sub>4</sub> measurements recorded during the releases selected  
for the inversions. The results indicate that over this range, the precision was < 20 ppb CH<sub>4</sub> and < 0.6 ppm  
195 CO<sub>2</sub> for the G2203 and G2401 analyzers, respectively, and that both analyzers still responded linearly ( $R^2$   
> 0.99) at high mole fraction values, with residual error between the gas analyzer response and the  
assigned values of lower than 2%.

The gas analyzers were installed in a Mitsubishi hybrid SUV vehicle. Measurements were made  
continuously at approximately 0.3-0.4 Hz while the vehicle was driven up and down the two main roads  
200 next to the TADI platform at a speed of about 10 km/h (~1 measurement every 7m) (Fig. 1). The distance  
between the release points and the car was between 25 m at the closest to about 250 m at the furthest.  
Due to the brevity of the releases, less than six cross-sections of the plume were identified in the mobile  
transects for each controlled release. The sampling inlet was located at the back of the vehicle  
approximately 2 m above the ground surface. The top of the sampling mast was equipped with a GPS  
205 providing a time reference along with measurement positions. At the beginning of the campaign, the  
overall time delay of the different analyzers, including the time delay induced by the sampling line and  
the analyzer time shift relative to GPS time, was empirically assessed by contaminating (breathing out)  
shortly at the air inlet at a given GPS time and comparing this time to the analyzer timestamp of the CO<sub>2</sub>  
response (at peak summit). The measurements were thus synchronized with 16s delay between the time a  
210 sample is taken at the sampling inlet and its recorded time with GPS receiver. Figure 2 shows an example  
of the transects on the TADI adjacent roadways, with observed instantaneous CH<sub>4</sub> mole fraction time  
series during a CH<sub>4</sub> release.

In the absence of a controlled tracer release, reliable measurements of the meteorological and turbulence  
parameters are essential to model the plumes from the releases with an atmospheric dispersion model. A  
215 meteorological station was installed and operated by TOTAL in the north-east of the ATEX zone (Figure  
1). This station included a Metek Sonic 3D sonic anemometer at 10 m height above the ground. The high  
frequency measurements of this anemometer were not recorded but combined at 1-minute resolution into  
mean horizontal wind speed ( $U$ ) and direction ( $\theta$ ), temperature ( $T$ ), Obukhov length ( $L$ ), surface friction  
velocity ( $u^*$ ), and standard deviation of wind velocity fluctuations ( $\sigma_u$ ,  $\sigma_v$ , and  $\sigma_w$ ). We averaged these 1-  
220 minute meteorological data over the entire release periods and used these as inputs for the modelling and



225

inversion configurations. Therefore, hereafter, the notations  $U$ ,  $\theta$ ,  $T$ ,  $L$ ,  $u^*$  and  $(\sigma_u, \sigma_v, \sigma_w)$  represent such averages over the release periods rather than the 1-minute data. All the releases were conducted during daytime under near-neutral or convective stability conditions ( $L < 0$ ). The atmospheric conditions during the whole campaign were dominated by prevailing low and highly variable winds of south-west to south-east origin.

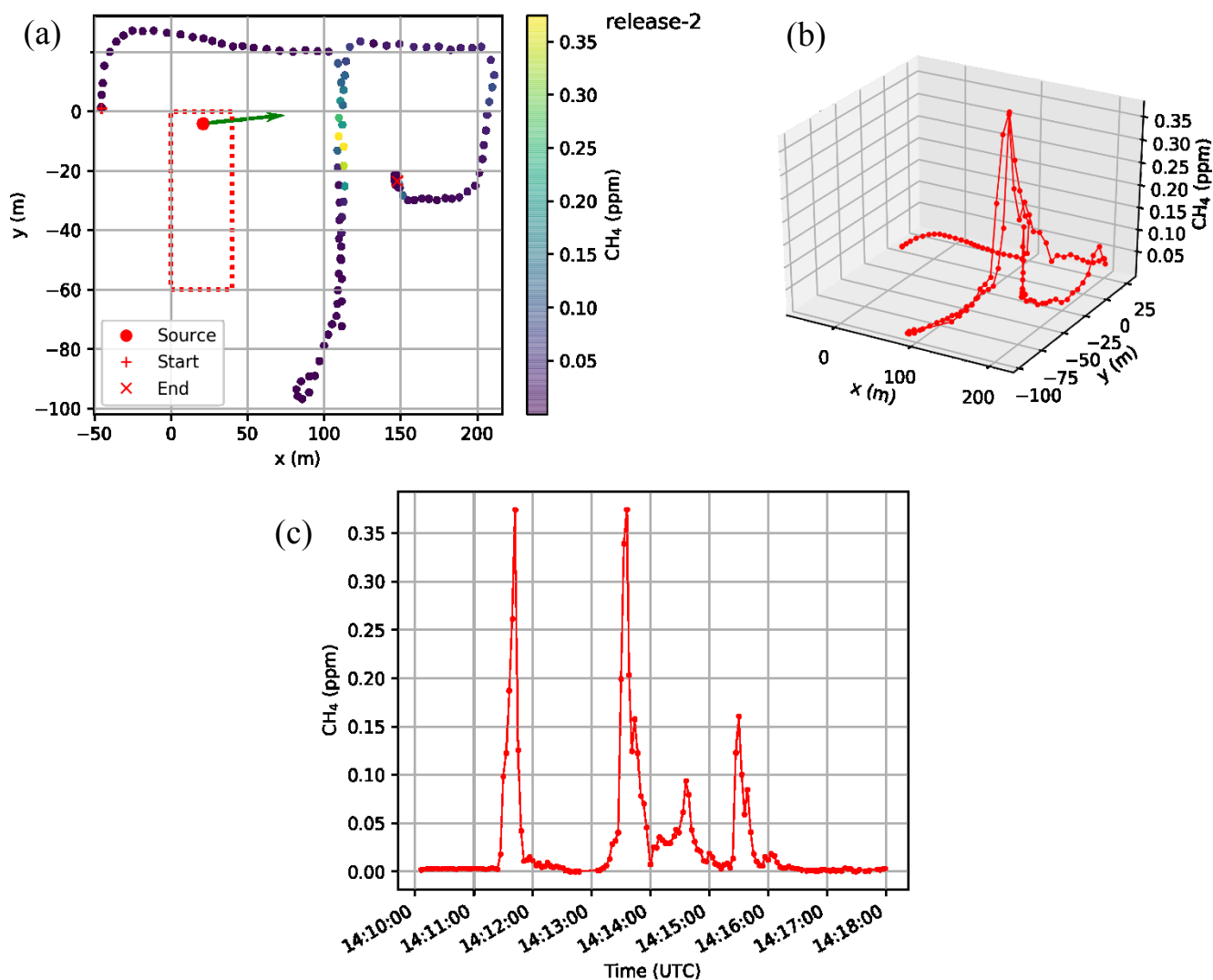


Figure 2: CH<sub>4</sub> mole fraction mobile measurements during CH<sub>4</sub> release no 2 (Table 2): (a) horizontal representation (b) 3D representation with values as a function of the horizontal location and (c) time series. The green arrow from the source location in (a) shows the averaged wind direction during that release.

230





### 3. Atmospheric inversion of the release locations and rates

#### 3.1 Gaussian plume dispersion model

235 The atmospheric inversion approach used here relies on a local scale Gaussian plume model to simulate the dispersion of CH<sub>4</sub> or CO<sub>2</sub> from the potential locations of the sources. Gaussian plume models (Hanna et al., 1982) provide an approximation of the average tracer dispersion on a local scale (source-receptor distances of less than a few kilometers) driven by constant meteorological conditions in time and space over a flat area. In such conditions, the concentration (*C*) of a pollutant has a distribution described by a combination of normal distributions in both vertical and horizontal planes. We use the following Gaussian  
240 model formulation assuming a reflective ground surface:

$$C(x, y, z) = \frac{Q_s}{2\pi\sigma_y\sigma_z U_e} \exp\left(\frac{-(y-y_s)^2}{2\sigma_y^2}\right) \left[ \exp\left(\frac{-(z-z_s)^2}{2\sigma_z^2}\right) + \exp\left(\frac{-(z+z_s)^2}{2\sigma_z^2}\right) \right] \quad (1)$$

where the *x* and *y* axis are defined by the effective wind direction, *Q<sub>s</sub>* is the emission rate of a point source located at (*x<sub>s</sub>*, *y<sub>s</sub>*, *z<sub>s</sub>*), *U<sub>e</sub>* is the effective mean wind speed at the height of a release, (*x*, *y*, *z*) are the coordinates of a receptor, and *σ<sub>y</sub>* and *σ<sub>z</sub>* are the dispersion coefficients in lateral (*y*) and vertical (*z*)  
245 directions, respectively. The dispersion coefficients *σ<sub>y</sub>* and *σ<sub>z</sub>* are derived from the standard deviations of the corresponding velocity fluctuations in the lateral (*σ<sub>v</sub>*) and the vertical (*σ<sub>w</sub>*) directions as follows (Gryning et al., 1987):

$$\sigma_y = \sigma_v t \left( 1 + \sqrt{\frac{t}{2T_y}} \right)^{-1} \quad (2a)$$

$$\sigma_z = \sigma_w t \left( 1 + \sqrt{\frac{t}{2T_z}} \right)^{-1} \quad (2b)$$

250 where *t* (*= x/U<sub>e</sub>*) is the travel time, *T<sub>y</sub>* and *T<sub>z</sub>* are the Lagrangian time scales in lateral (*y*) and vertical (*z*) direction, respectively. We take *T<sub>y</sub>* = 200s (Draxler, 1976) for near surface release and *T<sub>z</sub>* = 300s for unstable conditions (*L* < 0) (Gryning et al., 1987).

The small number of plume cross-sections (called “peaks” hereafter) observed in this study prevented us from assessing the average concentration along the roads where mobile transects were conducted for each  
255 release. Even though a Gaussian model characterizes the average plume under constant wind, and can thus deviate much from observed instantaneous plume cross-sections, we compared mole fractions simulated with such a model to the observed instantaneous mole fraction. A first reason is that one can hardly better match observed plumes using models simulating explicitly the turbulence since it is difficult



to capture the right timing and location of turbulent stochastic structures. Another reason is that the TADI  
260 platform is relatively flat and the very short duration of the releases prevented us from considering varying  
winds. Furthermore, our inversion method to localize the sources relies on a very high number of plume  
simulations that would not have been affordable with complex models. Finally, we consider the integral  
of the mole fractions above the background within cross-sections as the index of the plume amplitude  
whose observed value is fitted by the model in the inversion approach, which limits the impact of the lack  
265 of simulation of the turbulent patterns (Monster et al., 2014; Alberston et al., 2016; Ars et al, 2017).  
Therefore, the Gaussian model was assumed to be suitable to assimilate the information from our  
instantaneous plume cross-sections.

The wind conditions during the whole campaign with prevailing low wind speed and high variations of  
the direction challenges the spatial representativeness of the meteorological measurements and the use of  
270 local-scale dispersion models to simulate the peaks in the mobile transects. Such a limitation applies to  
Gaussian models as well as to more complex models, and, actually, our inversion approach attempts to  
take advantage of strong variations in the wind direction to localize the sources.

### 3.2 Inversion method

The inversion system primarily relies on the plume amplitudes (defined as the integral of the mole  
275 fractions above the background in peaks as in Ars et al. 2017; see section 3.1) along the mobile transects  
to infer the release rates. These amplitudes are the main component of the data assimilated by the  
inversion system. They highly depend on the distance from the source, whose location is unknown, to the  
measured peaks. The inversion scheme also follows the fact that, due to unsteady wind conditions and  
turbulence, the effective wind directions from the release point to the peaks in the mobile transects along  
280 the roads can differ from  $\theta$ , the mean wind direction averaged over the brief release periods. However,  
the variability of the wind measurements at high frequency should give a good indication of the  
fluctuations of such effective wind directions. This provides information about the source location so the  
position of the peaks along the mobile transects are the other component of the data assimilated by the  
inversion system. Crossing the information about the varying amplitude of the different peaks and of their  
285 location adds information about the source location, since the variations of the effective wind from a  
source to the roads impacts strongly the distance between the source and the peak, and thus, the peak  
amplitude.

In practice, in order to compare modeled peaks to measured ones, the inversion drives the Gaussian model  
with an effective wind direction  $\theta_m$  defined by the direction between the potential source locations and  
290 the peak locations, but with an effective wind speed and plume widths that are constrained with the  
meteorological measurements. More specifically,  $\theta_m$  is taken as the direction from the potential source  
location to the “center” of the measured peak. This center is estimated as the mid-point between the edges  
of the measured plume cross-sections, these edges being defined manually. If the estimate of  $\theta_m$  falls



outside the range of measured wind directions  $\theta \pm 2\sigma_\theta$ , (about 95% of the distribution around the average  
295 of the measured wind direction over a release period),  $\theta m$  is set to the corresponding maximum or  
minimum value ( $\theta \pm 2\sigma_\theta$ ), where  $\sigma_\theta$  is the standard deviation of the measured wind direction over a release  
period. Since the high frequency measurement of the wind were not recorded, for each release,  $\sigma_\theta$  is  
approximately calculated as  $\sigma_\theta \approx \sigma_v/U$  (Joffre and Laurila, 1987). The confidence in the  $\theta m$   
corresponding to a given source location is weighted by its relative departure from  $\theta$  compared to  $\sigma_\theta$ ,

300 We provide the actual source height of each release to the inversion system, which derives the unknown  
horizontal source location. The inversion discretizes the ATEX zone into small cells of  $1 \text{ m}^2$  to define all  
potential horizontal locations of the source. For each controlled release, looping over all these locations  
and on an extensive ensemble of values for the release rates with intervals of  $0.05 \text{ gX/s}$  (or of  $0.1 \text{ gX/s}$  if  
measurements at first sight indicate that the emission rate it is likely well above  $10 \text{ gX/s}$ , where  $X=\text{CH}_4$   
305 or  $\text{CO}_2$ ), the inversion algorithm determines the minimum of a cost function ( $J$ ) of these rates and  
locations, defined by:

$$J = J_p + J_w \quad (3)$$

where the first term:

$$J_p = \sum_{i=1}^{N_p} \left[ \frac{A\theta_i - Am_i}{A\theta_i} \right]^2 \quad (4)$$

310 is the quadratic sum of relative errors between the modeled ( $Am_i$ ) and observed ( $A\theta_i$ ) amplitudes of the  
 $N_p$  plume cross-sections (integrals of the mole fractions above the background between the edges of the  
observed peak that are defined manually) and the second term:

$$J_w = \sum_{i=1}^{N_p} \left[ \frac{\theta - \theta m_i}{\sigma_\theta} \right]^2 \quad (5)$$

315 is the quadratic sum the weighted departure of the implicit effective wind directions  $\theta m_i$  corresponding  
to the  $N_p$  peaks from  $\theta$ , the mean wind direction over the release period.

The estimates of the unknown location ( $x_e, y_e$ ) and rate ( $Q_e$ ) of each release are taken as the values  
corresponding to the minimum of the cost function  $J$ .  $J_w$  weights the departure of  $\theta m$  from  $\theta$  using  $\sigma_\theta$ ,  
which characterizes here the uncertainty in the effective winds. However, the misfits between modeled  
and simulated peak amplitudes (Eq. 4) are not weighted by the uncertainty in the transport model.  
320 Actually, the direct comparison of  $J_w$  and  $J_p$  in  $J$  implicitly assumes that there is a 100% uncertainty in  
the skill of the model to simulate the amplitude of individual peaks when feeding it with the actual release  
locations and rates, which is a rather conservative assumption (Ars et al. 2017).

The first results analyzed based on the inversion configuration described above and presented in sections  
5.1 and 5.2 have led us to conduct some tests of sensitivity of the results: (1) by fixing the location of the



325 source to its actual position and minimizing  $J_p$  to get an estimate of the release rates (2) by modifying the  
formulation of  $J_p$  to influence the way it weights the fit to the different peaks (see section 5.3). Section 5  
details these tests and their results.

## 4. Data analysis for the configuration of the transport model and inversion

### 4.1 Assignment of the background mole fractions

330 The definition of the background field of CH<sub>4</sub> or CO<sub>2</sub> for the measured peaks can have a strong impact  
on the derivation of the peak amplitudes in the measurement transects. Our modeling framework includes  
the Gaussian simulation of the plumes from the controlled releases but not a simulation of the background  
mole fractions over which the plumes represent an excess of CH<sub>4</sub> or CO<sub>2</sub>. We compute a single  
background value per release. During CH<sub>4</sub> releases, we define the background for each release as the  
335 minimum of the corresponding measured CH<sub>4</sub> mole fraction time series. Indeed, the variations of CH<sub>4</sub>  
between the peaks that are unambiguously attributed to the release plume appear to be quite negligible in  
most cases, which can be explained by the short duration of the releases. However, the concentrations  
were much noisier between the peaks in the CO<sub>2</sub> mobile transects, due to potential sources and sinks of  
CO<sub>2</sub> nearby such as vegetation and traffic (e.g. delivery trucks passing frequently along the road  
340 surrounding the TADI platform). Therefore, we define the CO<sub>2</sub> background value for a given CO<sub>2</sub> release  
as the 5<sup>th</sup> percentile of the corresponding measured CO<sub>2</sub> mole fraction time series. These background  
values are subtracted from the measurement timeseries for the comparisons to the Gaussian model  
outputs.

### 4.2 Configuration of the Gaussian model and identification of the releases for which the modeling 345 framework is suitable

We use the average of the 1-minute data from the Metek 3D sonic anemometer over each release period  
as inputs to the Gaussian plume model: the average of the standard deviations of velocity fluctuations in  
the lateral ( $\sigma_v$ ) and the vertical ( $\sigma_w$ ) directions are used to compute the dispersion parameters  $\sigma_y$  and  $\sigma_z$ ,  
and the average wind speed  $U$  is taken as the effective wind speed  $U_e$  driving the Gaussian model.

350 The inversion method relies on the detection and use of clear peaks in the gas mole fraction timeseries  
that really correspond to plume cross-sections from one edge to the other edge of the plumes. Several  
peaks in the measurements were associated to situations for which the vehicle had to turn (e.g. at the  
crossing of roads) and thus did not fully cross the plumes. Such peaks are not retained for the inversions.  
Furthermore, some peaks were measured at locations very far from the area along the road corresponding  
355 to the projection of the ATEX zone with the  $\theta \pm 2\sigma_\theta$  range of wind directions. The reliability in inversions  
using such peaks would be very low and we thus exclude all peaks for which the difference between the  
corresponding  $\theta_m$  and  $\theta$  systematically exceeds 30° whichever location is tested for the source. Due to



the complex meteorological conditions during the campaign (60% of the release were conducted while the wind was lower than  $2 \text{ ms}^{-1}$ ), the low number of detected peaks and such a selection of the suitable ones for inversion did not leave any exploitable peak for 34 of the controlled releases. Only seven  $\text{CH}_4$  and nine  $\text{CO}_2$  releases were thus selected for the inversions (Table 2). This selection of releases narrows a bit the range of release rates tested during the TADI-2018 campaign, but the resulting range (0.3 to  $45 \text{ gCH}_4/\text{s}$  and 2 to  $150 \text{ gCO}_2/\text{s}$ , see Table 2) still spans three orders of magnitude.

About 30% of these releases were conducted in weak wind speed conditions, with  $U < 2 \text{ ms}^{-1}$ , which are usually assumed to be challenging for local dispersion modeling (Wilson et al., 1976). Such conditions are associated with complex dispersion patterns of the gases released, and deviate from the validity range of the Gaussian plume dispersion model. We still analyze these releases, but our confidence *a priori* in these results is thus weaker than for the other releases and specific statistics will be derived in section 5 for cases when  $U \geq 2 \text{ ms}^{-1}$ .

In releases nos. 5 and 6, part of the mole fractions measured in the plume cross sections (3% and 10% respectively) reach values above the CRDS analyzer's recommended range (above 20ppm, see section 2.2), with maximum values of  $\sim 60\text{ppm}$  and  $\sim 85\text{ppm}$  respectively. These are the only releases selected for inversion for which measurements were out of this range. Table 2 provides information about the corresponding release rate, number of peaks, and meteorological parameters. Meteorological observations were missing for the two last releases due to technical problems (for release nos. 15 and 16 in Table 2). For these two releases, meteorological observations from the previous release (i.e. no. 14) which occurred about nine minutes before are used for the inversion. For the selected releases which correspond to low wind conditions ( $U < 2 \text{ ms}^{-1}$ ), we set a minimum value of  $0.3 \text{ ms}^{-1}$  for  $\sigma_v$ , and the effective wind speed of the Gaussian model to  $U_e = (U^2 + 2\sigma_v)^{1/2}$  (Qian and Venkatram, 2011). Atmospheric stabilities during the selected releases were in the range of neutral to very unstable as all the gas releases were conducted during day time and the observed values of  $L$  were negative (Table 2).

Table 2: Releases to which the inversion is applied, with the corresponding release duration, actual release rate ( $Q_s$ ), number of peaks in the mobile measurement transects, and averaged values of the meteorological and turbulence parameters over the release period.

Release no.	Gas	Duration (mm:ss)	No. Peaks	$Q_s$ (g/s)	$z_s$ (m)	$U$ (m/s)	$\theta$ (°)	$l/L$ ( $\text{m}^{-1}$ )	$u^*$ (m/s)	$\sigma_u$ (m/s)	$\sigma_v$ (m/s)	$\sigma_w$ (m/s)
1	$\text{CH}_4$	07:48	2	1	2.3	2.06	294.8	-0.03	0.34	0.55	0.60	0.50
2	$\text{CH}_4$	06:54	2	0.5	2.1	2.64	290.7	-0.06	0.26	0.42	0.50	0.42





3	CH <sub>4</sub>	18 :25	6	0.3	2.1	2.86	285.7	-0.08	0.23	0.48	0.41	0.42
4	CH <sub>4</sub>	08:36	4	0.5	7.0	2.90	312.6	-0.02	0.31	0.49	0.50	0.42
5	CH <sub>4</sub>	08:31	4	45	1.6	2.29	307.4	-0.06	0.22	0.40	0.48	0.37
6	CH <sub>4</sub>	14:25	4	3	1.1	1.77	156.3	-0.04	0.22	0.41	0.41	0.38
7	CH <sub>4</sub>	12:00	2	0.5	2.6	2.40	142.7	-0.02	0.23	0.44	0.32	0.32
8	CO <sub>2</sub>	06:18	2	150	1.6	3.32	67.42	-0.01	0.37	0.67	0.58	0.48
9	CO <sub>2</sub>	08:57	2	5	1.7	3.31	76.7	-0.01	0.38	0.77	0.67	0.54
10	CO <sub>2</sub>	06:39	4	3	0.6	2.85	55.7	-0.01	0.28	0.49	0.52	0.41
11	CO <sub>2</sub>	04:49	2	2	1.9	2.19	52.1	-0.01	0.25	0.39	0.44	0.35
12	CO <sub>2</sub>	04:20	1	150	1.6	1.23	312.2	-0.09	0.17	0.25	0.27	0.28
13	CO <sub>2</sub>	04:30	2	85	1.6	1.41	304.5	-0.04	0.22	0.28	0.29	0.32
14	CO <sub>2</sub>	04:01	2	60	1.6	1.26	308.1	-0.16	0.19	0.34	0.31	0.28
15	CO <sub>2</sub>	04:52	2	30	1.6	1.26	308.1	-0.16	0.19	0.34	0.31	0.28
16	CO <sub>2</sub>	04:00	3	10	1.6	1.26	308.1	-0.16	0.19	0.34	0.31	0.28

## 5. Results

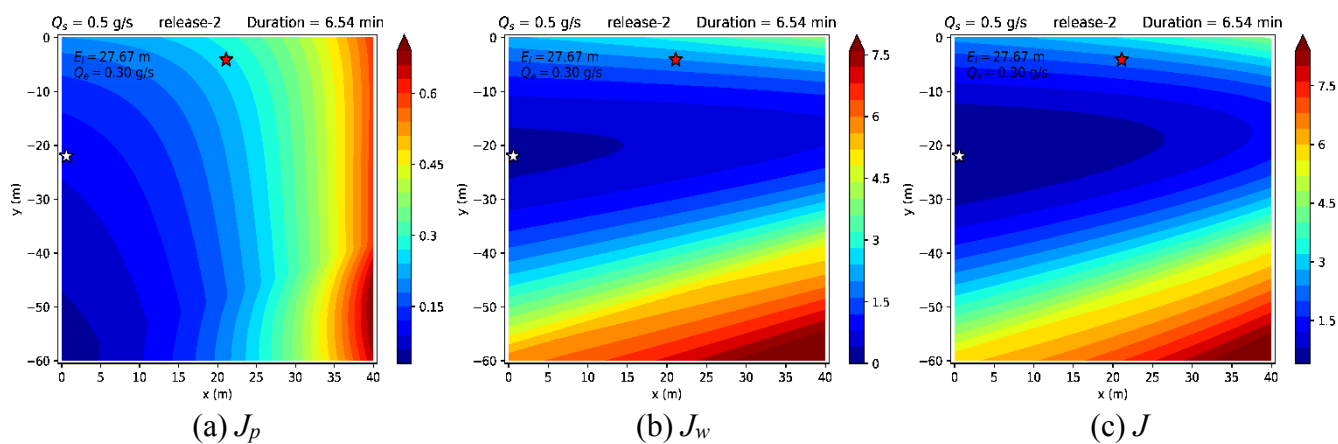
We evaluate the inversion estimates of the rates and locations of the selected releases using the actual values provided by TOTAL. The number of plume cross-sections used by the inversion for individual CH<sub>4</sub> or CO<sub>2</sub> releases varies from 1 to 6 with a typical range of 2-4 (Table 2).

### 5.1 CH<sub>4</sub> releases

Table 3 shows the inverted and actual release rates and location errors for the seven CH<sub>4</sub> releases. As an example, the shape as a function of the source location within the ATEX zone and the minimum of the cost function  $J$  (and of its components  $J_p$ , and  $J_w$ ) are illustrated by fixing the release rate to its inversion estimate, and compared to the actual position of the source for the release no 2 in Figure 3. This Figure,



400 highlights the dominant role of  $J_w$  in the determination of the source location. For this release, Figure 4 also shows a comparison between the observed and modeled (using the source location and rate given by the inversion) CH<sub>4</sub> mole fraction peaks for two of the plume cross-sections. For both cross-sections, the maxima of the measurements are larger than that of the modeled mole fractions but the modeled plume cross-section is wider, as explained by the use of a Gaussian model which is representative of the average dispersion. However, the modeled and observed integral of the mole fractions above the background within the plume cross-sections agree within 25%. The average of this relative difference between simulated and observed peak amplitudes (comparing the absolute value of the differences to the observed amplitude) over all peaks from all releases is about 43%. The deviation of  $\theta_m$  from  $\theta$  varies from less than 1° to ~16° with average deviation of ~7° over all the peaks in all CH<sub>4</sub> releases, while  $\sigma_\theta$  varies 405 between 8° and 17°, with an average value of 11°. These values explain that at the inversion optimal release location and rate estimates, the value of  $J_p$  is smaller than that of  $J_w$  (as illustrated in Fig. 3).



410 Figure 3: Contour plots of (a)  $J_p$ , (b)  $J_w$ , and (c)  $J$  when fixing the release rate to its inverted value  $Q_e$  for release no 2. Red and white stars respectively show the actual and inverted source locations.

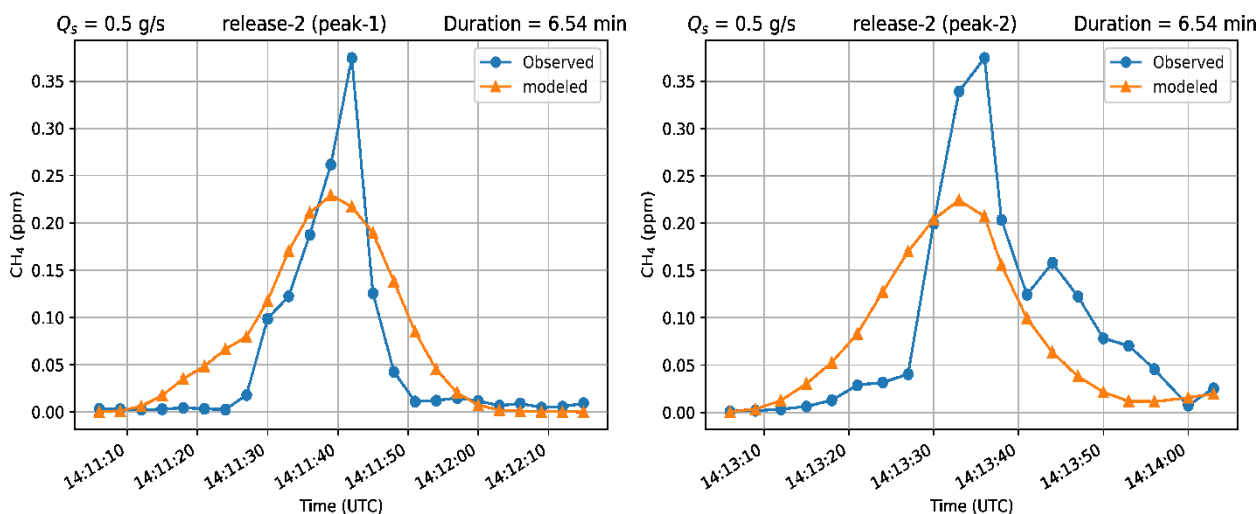


Figure 4: Observed and modeled CH<sub>4</sub> mole fraction peaks for two plume cross-sections used in the inversion for release no 2 using the source location and rate estimates from the inversion.

415 For each controlled release, the error in retrieved source location (“location error” hereafter)  $E_l$  is defined  
by the Euclidean distance between the inverted and actual source. It varies from 8.1 m to 62.9 m, with an  
average value of 29.8 m, across all the selected CH<sub>4</sub> releases. Figure 5(a) shows a comparison between  
the estimated and actual release rates for these releases. The relative estimation error for the release rates  
(dividing the absolute value of the estimation error by the actual emission rate) varies from less than 10%  
420 (for release no. 4) to ~82% (for release no. 5) (Table 3, Figure 5(a)). These results indicate that the  
inversions lead to an average relative error of 30.8% in the release rate. In most of the cases, the estimates  
of the rates are within a factor of 1.9 from the actual ones, except for release no 5, for which the actual  
release rate is underestimated by a factor of 5.5. The underestimation of emission in release no. 6 is the  
second-worst case with ~47% relative error. The small percentage of mole fractions measured above the  
425 analyser’s operational range for CH<sub>4</sub> during releases no. 5 and 6 (section 4.2) hardly explains that these  
releases correspond to the poorest results. Selecting the cases for which  $U \geq 2 \text{ ms}^{-1}$  slightly decreases the  
average relative error to 28%, release no. 6 being the only one for which  $U < 2 \text{ ms}^{-1}$ . However, ignoring  
the results for the worst case (release no. 5), the average relative error in the release rate is ~22%. In most  
of the cases, the actual release rates are underestimated by the inversion (release no. 4 and 7 being  
430 exceptions).



Table 3: Summary of the inversion results with comparisons between the actual and inverted source locations and rates for the CH<sub>4</sub> releases.

Release no.	Gas	$Q_s$ (g/s)	Inversions minimizing $J$ (Eq. (3))			Inversions minimizing $J^{log}$ (Eq. (7))		
			$Q_e$ (g/s)	Rel. error	$E_l$ (m)	$Q_e$ (g/s)	Rel. error	$E_l$ (m)
1	CH <sub>4</sub>	1	0.8	20.0%	26.8	1.05	5.0%	26.8
2	CH <sub>4</sub>	0.5	0.3	40.0%	27.7	0.3	40.0%	27.7
3	CH <sub>4</sub>	0.3	0.25	16.7%	21.5	0.25	16.7%	21.5
4	CH <sub>4</sub>	0.5	0.5	0.0%	8.1	0.6	20.0%	7.7
5	CH <sub>4</sub>	45	8.05	82.1%	38.8	9.05	79.9%	38.8
6	CH <sub>4</sub>	3	1.6	46.7%	62.9	3.3	10.0%	62.9
7	CH <sub>4</sub>	0.5	0.55	10.0%	23.2	0.75	50.0%	23.2

435

## 5.2 CO<sub>2</sub> releases

The general patterns and relative weight of  $J_w$  and  $J_p$  for CO<sub>2</sub> releases is similar to that for CH<sub>4</sub> releases. The average relative difference between modeled and observed peak amplitudes is about 31%. The deviation of  $\theta_m$  from  $\theta$  varies from less than 1° to ~26° with an average value of ~7° over all the peaks in all CO<sub>2</sub> releases, while  $\sigma_\theta$  varies from 10° to 22° with an average value of 13°. Again, this is associated with lower values for  $J_p$  than  $J_w$  (not shown).

440

Table 4 and Figure 5(b) compare the estimate of the CO<sub>2</sub> releases rates and locations to their actual values. The location error is, on average, ~39 m. For all the 9 CO<sub>2</sub> releases that have been analyzed, the emissions are estimated within a factor of 1.4 of the actual emissions. The relative error in the release rate estimates varies from less than 2% (release 10) to 28.6% (release 8), and, on average is 17.2%. Ignoring the four releases corresponding to  $U < 2\text{ms}^{-1}$ , the average relative error for the estimate of release rates significantly decreases to 11.6%. As for CH<sub>4</sub> releases, there is a general tendency of the inversions to underestimate the actual release rates (with two exceptions: release no. 10 and 12).

445

450

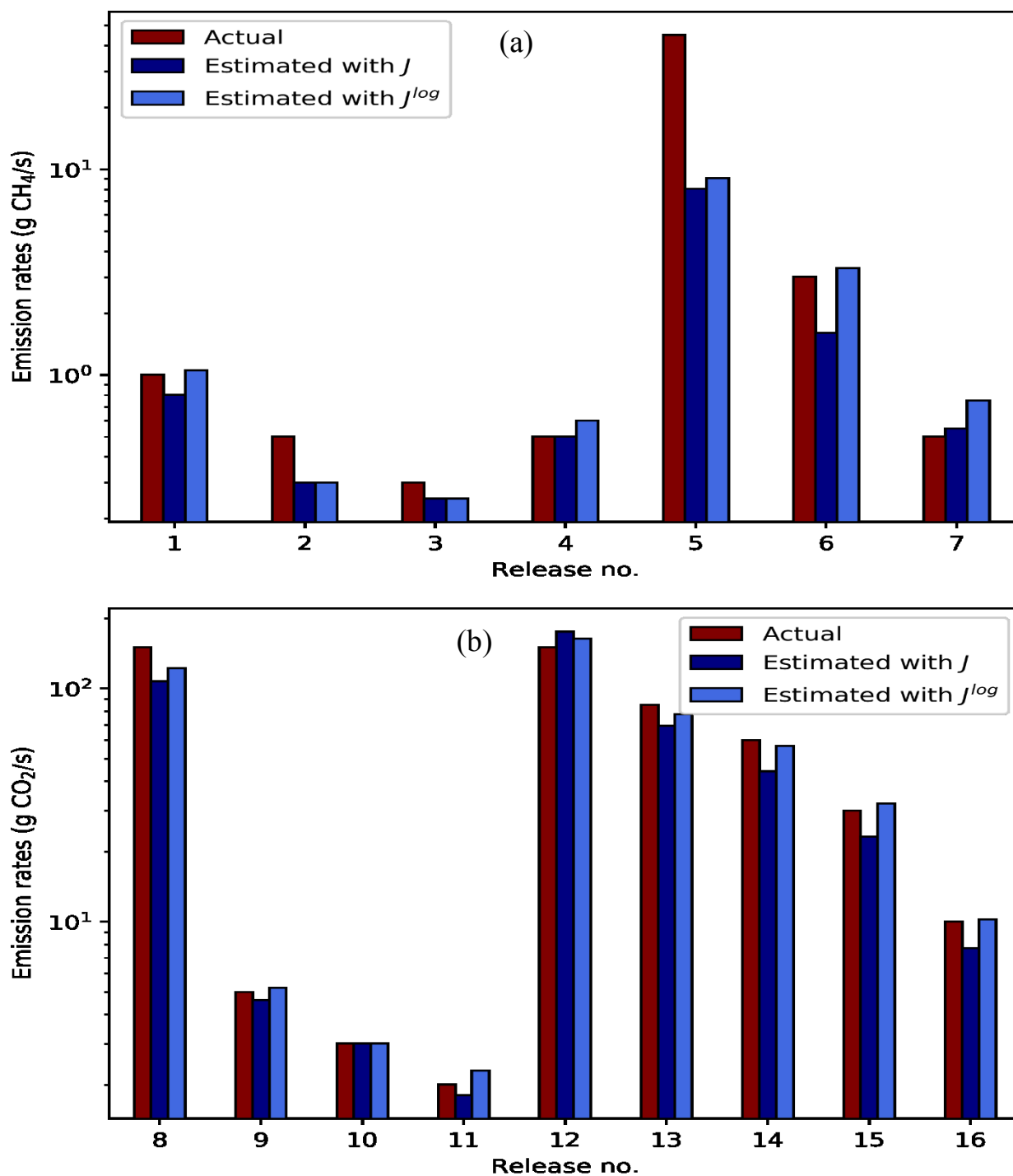


Figure 5: Comparison of the estimated and actual emissions rates of (a) CH<sub>4</sub> and (b) CO<sub>2</sub> releases.





Table 4: Summary of the inversion results with comparisons between the actual and inverted source location and rates for CO<sub>2</sub> releases.

Release no.	Gas	$Q_s$ (g/s)	Inversions minimizing $J$			Inversions minimizing $J^{log}$		
			$Q_e$ (g/s)	Rel. error	$E_l$ (m)	$Q_e$ (g/s)	Rel. error	$E_l$ (m)
8	CO <sub>2</sub>	150	107.1	28.6%	21.5	122.1	18.6%	21.5
9	CO <sub>2</sub>	5	4.6	8.0%	43.9	5.2	4.0%	43.9
10	CO <sub>2</sub>	3	3.0	0.0%	32.3	3.0	0.0%	33.2
11	CO <sub>2</sub>	2	1.8	10.0%	56.4	2.3	15.0%	60.9
12	CO <sub>2</sub>	150	175.1	16.7%	26.1	163.6	9.1%	23.3
13	CO <sub>2</sub>	85	69.1	18.7%	44.8	77.6	8.7%	44.8
14	CO <sub>2</sub>	60	44.1	26.5%	44.8	56.6	5.7%	44.8
15	CO <sub>2</sub>	30	23.1	23.0%	44.8	32.1	7.0%	44.8
16	CO <sub>2</sub>	10	7.7	23.0%	39.6	10.2	2.0%	39.6

455

### 5.3 Least square fitting of the order of magnitude of the peak amplitudes rather than of their values: a sensitivity test

The results for both CH<sub>4</sub> and CO<sub>2</sub> releases indicate that for ~90% of the cases, the release rates are underestimated by the inversion. However, the locations of the sources are generally found to be too far from the main measurement transects compared to their actual position, an inversion bias which should rather lead to an overestimation of the release rates. Experiments using the same inversion framework but fixing the source location to its actual position (minimizing  $J_p$ ) leads to a ~44% and ~33% average relative error in the estimate of the CH<sub>4</sub> and CO<sub>2</sub> release rates respectively, i.e. to larger errors. Actually, the underestimation of the release rates coincides with the underestimation of most of the peak amplitudes. Across the different peaks corresponding to a given release, the relative difference between simulated and observed plume amplitude is highly variable and it appears that the system is often highly sensitive to one or two peaks for which it provides a slight overestimation, balanced by a large underestimation of the other peaks.

A potential explanation for the overestimation of the distance to the source and for the underestimation of the release rates is thus that the term  $J_p$  of the cost function does not push enough for finding a source location and rate providing a good fit to most of the peak amplitudes. In particular, it does not push enough



for getting the right variations in terms of peak amplitude from one plume cross-section to the other. With such a lack of constraint regarding the relative amplitude of the different peaks, and with values for  $J_p$  much lower than those for  $J_w$ , a primary driver of the minimization of  $J$  is that of  $J_w$  by localizing the source as far as possible.

Therefore, a sensitivity test is performed to put more emphasis on a better fit to the different peak amplitudes and to loosen the strongest constraints towards specific peaks. The term  $J_p$  is modified to weight the misfits between the modeled and measured amplitudes of the plume cross-sections in terms of order of magnitude using a logarithmic scale:

$$J_p^{log} = \sum_{i=1}^P \left[ \frac{\log(1+Ao_i) - \log(1+Am_i)}{\log(1+Ao_i)} \right]^2 \quad (6)$$

In a new series of estimations, the inversion minimizes

$$J^{log} = J_p^{log} + J_w \quad (7)$$

instead of  $J$ . The corresponding results (Tables 3&4 and Figure 5) are slightly better than that obtained when minimizing  $J$ .

Minimizing  $J^{log}$  for the CH<sub>4</sub> releases, the location errors vary from 7.7 m to 62.9 m, with an average value of 29.8 m (Table 3) and the relative error in the estimates of the release rate vary from ~5% (release no 1) to ~80% (release no 14), with a ~31% average value. These scores are very similar to that when minimizing  $J$ . Minimizing  $J^{log}$  for the CO<sub>2</sub> releases, the average location error is 39.6m, which, again, is similar to the average location error when minimizing  $J$ . However, there is a significant improvement in the estimate of the CO<sub>2</sub> release rates when minimizing  $J^{log}$ : the relative error in this estimate varies from less than 2% to 18.6%, with an average relative error of 7.8%. For all the nine CO<sub>2</sub> releases, minimizing  $J^{log}$  leads to release rate estimates within a factor of 1.2 of the actual release rates.

A more general improvement when minimizing  $J^{log}$  is that there is no general tendency to underestimate the release rates, with now 60% of cases for which the release rate is actually over-estimated. However, the tendency to overestimate the distance of the source from the main mobile measurements transects persists. This reveals that a tendency of the system to lead to the underestimation of the release rates also persists even if it is decreased, but that it is now better balanced by its opposed tendency to increase the release rates to compensate for the location of the source too far from the plume cross-sections. Indeed, fixing the source location to its actual position, the minimization of  $J_p^{log}$  leads, as the minimization of  $J_p$ , to a general tendency to underestimate the release rates (and to a ~37% -respectively ~27%- relative error in the estimate of the CH<sub>4</sub> -respectively CO<sub>2</sub>- release rates).



## 6. Discussion

505 Our inversion system can provide estimates of the CH<sub>4</sub> and CO<sub>2</sub> release rates with a 20%-30% relative errors over a wide range of rates tested during the TADI campaign. The more complex background conditions during the CO<sub>2</sub> releases did not appear to be a limitation for the inversion which provided more precise estimates of the CO<sub>2</sub> releases than of the CH<sub>4</sub> releases on average. An important driver of the release rate inversion precision appeared to be the meteorological conditions. Even though the estimates for low wind speed were not associated to much larger estimation error, the specific variations of the wind for each release appears to play a critical role in the ability to fit the various amplitudes of the plume cross-sections. The particularly challenging meteorological conditions encountered during the campaign limited the skill of the inversion to retrieve the location of the releases. But the system still achieved a ~30-40m precision for such an estimation with measurements taken at 50-150m most of the time.

515 Our results and inversion approach appear to be promising given the very complex conditions of the campaign with very brief releases and very low but highly varying wind conditions. Longer release durations e.g. at least 30 minutes would provide a much higher number of plume cross-sections around the site and ensure much more favorable inversion conditions. Previous studies dedicated to the estimate of release rate from point source using mobile measurement across the plumes and atmospheric dispersion models (such as Brantley et al., 2014; Foster-Wittig et al., 2015; Albertson et al., 2016) also documented typical average precisions of 20-30% but they relied on releases and measurement timeseries lasting at least 20 minutes. Caulton et al. (2018) recommend to use at least 10 plume cross-sections to reliably constrain atmospheric variability and reduce the uncertainties in the estimation of emission rate using mobile measurements. However, our results demonstrate that we can achieve a good estimation precision with a much smaller number of plume cross-sections.

Some major improvements can be foreseen to strengthen the measurement and inversion framework. The general tendency of the transport and inversion framework to underestimate the release rates (compensated by its tendency to overestimate the distance between the source and the plume cross-sections when using a logarithmic cost function) can actually be related to the source height (Yacovitch et al., 2020). In the inversion computations, this height is fixed to the actual source height for the controlled releases. However, the gas is released with significant velocity and difference of temperature relative to the ambient environment, leading to some important rise up of the plume to several meters above the actual release point. Images taken with hyperspectral cameras by other participants in the TADI campaign during some of the releases indicate that the released plume had significant momentum which caused it to rise by approximately 2-3m (likely up to 10 m for some releases) above the actual release points. An effective injection height accounting for plume rising (Briggs, 1975) may thus have to be considered in the model. In principle, the inversion could optimize the injection height as well as the release location and rate. However, the problem would be too underconstrained for the TADI campaigns



540 given the limited number of plume cross-sections for each release, and thus, because of the brevity of the release.

Uncertainties in the atmospheric stability and other meteorological and turbulence parameters can be a critical source of errors, especially when targeting short releases. Here, the parameterization of the Gaussian model relied on meteorological turbulence measurements that can be poorly representative of the atmospheric conditions from the location of the release to the measurement sections for some releases.  
545 Using the integral of the gas mole fractions within the plume cross-sections as observation limits the impact of uncertainties in the horizontal diffusion. However, the vertical dispersion is generally more important than the horizontal dispersion and uncertainties in vertical dispersion can significantly impact the inversion of the release rate (Caulton et al., 2018). The strong underestimation of the CH<sub>4</sub> emission in release no 5 is probably due to a poor representation of the atmospheric stability conditions. Mobile  
550 measurement taken at different heights simultaneously could help overcome such an issue.

A better assessment of the model errors without using the knowledge on the actual source rate and location (potentially with the kind of techniques envisaged in Ars et al., 2017) could also help refine the definition of  $J_p$ . The conservative assumption regarding this error that is implicitly made in Eq (4) partly explains that  $J$  is dominated by  $J_w$  and thus the lack of fit to the different plume cross-section during a given release.  
555 More sensible estimations of the skill of the model to simulate the amplitude of the peaks lower than 100% could be used to increase the weight of departure from the observed amplitude.

As mentioned earlier, many of the releases during the TADI campaign were conducted under weak wind conditions. The Gaussian plume models have limited applicability in such weak wind conditions (Thomson and Manning, 2000) even though they are shown to provide reasonable dispersion simulations  
560 under moderate to strong wind conditions. For practical reasons, the selection of the Gaussian model, fast and relatively easy to implement and control, appeared to be optimal for the initial tests of the inversion framework and to simulate plumes for a very wide range of potential source locations in the inversion scheme. However, more advanced models like Lagrangian dispersion models and/or Computational Fluid  
565 Dynamics (CFD) models are more suitable for atmospheric dispersion in such extreme meteorological conditions (Tominaga and Stathopoulos, 2013). Combining such models with our inversion approach could provide opportunities to account for the variations of the wind in space and time and for vertical profiles of the releases. However, due to the computational cost of such models, they may be difficult to use for the inversion of the source location. A hybrid approach combining both types of model for the joint inversion of the source location and rate might be a solution to this problem.

## 570 7. Conclusions

In this study, a simple atmospheric inversion modeling framework was developed for localization and quantification of unknown CH<sub>4</sub> and CO<sub>2</sub> emissions from point sources based on mobile concentration



measurements. The inversion framework relies on a local-scale Gaussian plume dispersion model and it exploits the position and amplitude of the different mole fraction peaks to infer the source locations and rates. We used it to analyze a series of experiments with very brief controlled release of CH<sub>4</sub> and CO<sub>2</sub> with a wide range of rates during the TADI-2018 campaign. These releases were detected and quantified using a series of mobile measurement transects across the corresponding plumes made with instruments onboard a car that drove along roads around the emission area. Results indicate a 20-30% average error on the estimate of the release rates, and ~30-40m errors in the estimates of the release locations. Considering the challenging transport and emission conditions during the TADI-2018 campaign, the limited number of plume cross-sections (typically 2-4) per release, and the limitations of the Gaussian dispersion modeling framework for short duration to simulate instantaneous mole fractions, these good inversion results for both CH<sub>4</sub> and CO<sub>2</sub> releases appear to be encouraging.

## 585 Acknowledgements

This work was supported by the Chaire Industrielle Trace ANR-17-CHIN-0004-01 co-funded by the ANR French national research agency, TOTAL-Raffinage Chimie, SUEZ, and THALES ALENIA SPACE.

## References

- 590 Albertson, J.D., Harvey, T., Foderaro, G., Zhu, P., Zhou, X., Ferrari, S., Amin, M.S., Modrak, M., Brantley, H. and Thoma, E.D., 2016. A mobile sensing approach for regional surveillance of fugitive methane emissions in oil and gas production. *Environmental science & technology*, 50(5), pp.2487-2497.
- Alvarez, R.A., Zavala-Araiza, D., Lyon, D.R., Allen, D.T., Barkley, Z.R., Brandt, A.R., Davis, K.J., Herndon, S.C., Jacob, D.J., Karion, A. and Kort, E.A., Lamb, B.K., Lauvaux, T., Maasackers, J.D., Marchese, A.J., Omara, M., Pacala, S.W., Peischl, J., Robinson, A.L., Shepson, P.B., Sweeney, C., Townsend-Small, A., Wofsy, S.C., Hamburg, S.P., 2018. Assessment of methane emissions from the US oil and gas supply chain. *Science*, 361(6398), pp.186-188.
- Ars, S., 2017. Caractérisation des émissions de méthane à l'échelle locale à l'aide d'une méthode d'inversion statistique basée sur un modèle gaussien paramétré avec les données d'un gaz traceur. *Météorologie*. Université Paris-Saclay, Français. <NNT: 2017SACLV030>. <tel-01624241>
- 600 Ars, S., Broquet, G., Kwok, C.Y., Roustan, Y., Wu, L., Arzoumanian, E. and Bousquet, P., 2017. Statistical atmospheric inversion of local gas emissions by coupling the tracer release technique and local transport modelling: a test case with controlled methane emissions. *Atmospheric Measurement Techniques*, 10, 12, 5017-5037.





- 605 Brantley, H.L., Thoma, E.D., Squier, W.C., Guven, B.B. and Lyon, D., 2014. Assessment of methane emissions from oil and gas production pads using mobile measurements. *Environmental science & technology*, 48(24), pp.14508-14515.
- Briggs, G.A. (1975): Plume rise predictions. Lectures on Air Pollution and Environmental Impact Analyses, Workshop Proceedings, Boston, Massachusetts. September 29-October 3. pp. 59-111,  
610 American Meteorological Society, Boston, Massachusetts.
- Cartwright, L., Zammit-Mangion, A., Bhatia, S., Schroder, I., Phillips, F.A., Coates, T., Negandhi, K., Naylor, T.A., Kennedy, M., Zegelin, S. and Wokker, N., 2019. Bayesian atmospheric tomography for detection and quantification of methane emissions: application to data from the 2015 Ginninderra release experiment. *Atmos. Meas. Tech.*, 12, 4659-4676
- 615 Caulton, D.R., Li, Q., Bou-Zeid, E., Fitts, J.P., Golston, L.M., Pan, D., Lu, J., Lane, H.M., Buchholz, B., Guo, X. and McSperritt, J., 2018. Quantifying uncertainties from mobile-laboratory-derived emissions of well pads using inverse Gaussian methods. *Atmospheric Chemistry and Physics*, 18(20), pp.15145-15168.
- Caulton, D.R., Shepson, P.B., Cambaliza, M.O., McCabe, D., Baum, E. and Stirm, B.H., 2014. Methane destruction efficiency of natural gas flares associated with shale formation wells. *Environmental science & technology*, 48(16), pp.9548-9554.  
620
- Draxler, R.R., 1976. Determination of atmospheric diffusion parameters. *Atmospheric Environment* (1967), 10(2), pp.99-105.
- Duren, R.M., Thorpe, A.K., Foster, K.T., Rafiq, T., Hopkins, F.M., Yadav, V., Bue, B.D., Thompson, D.R., Conley, S., Colombi, N.K. and Frankenberg, C., 2019. California's methane super-emitters. *Nature*,  
625 575(7781), pp.180-184.
- Feitz, A., Schroder, I., Phillips, F., Coates, T., Negandhi, K., Day, S., Luhar, A., Bhatia, S., Edwards, G., Hrabar, S. and Hernandez, E., 2018. The Ginninderra CH<sub>4</sub> and CO<sub>2</sub> release experiment: An evaluation of gas detection and quantification techniques. *International Journal of Greenhouse Gas Control*, 70, pp.202-224.
- 630 Foster-Wittig, T.A., Thoma, E.D. and Albertson, J.D., 2015. Estimation of point source fugitive emission rates from a single sensor time series: A conditionally-sampled Gaussian plume reconstruction. *Atmospheric Environment*, 115, pp.101-109.
- Frankenberg, C., Thorpe, A.K., Thompson, D.R., Hulley, G., Kort, E.A., Vance, N., Borchardt, J., Krings, T., Gerilowski, K., Sweeney, C. and Conley, S., 2016. Airborne methane remote measurements reveal  
635 heavy-tail flux distribution in Four Corners region. *Proceedings of the national academy of sciences*, 113(35), pp.9734-9739.



- Goetz, J.D., Avery, A., Werden, B., Floerchinger, C., Fortner, E.C., Wormhoudt, J., Massoli, P., Herndon, S.C., Kolb, C.E., Knighton, W.B. and Peischl, J., 2017. Analysis of local-scale background concentrations of methane and other gas-phase species in the Marcellus Shale. *Elem Sci Anth*, 5.
- 640 Gryning, S. E., Holtslag, A. A. M., Irwin, J. S. and Sivertsen, B.: Applied dispersion modelling based on meteorological scaling parameters, *Atmos. Environ.*, 21(1), 79–89, doi:10.1016/0004-6981(87)90273-3, 1987.
- Hanna, S. R., Briggs, G. A., and Hosker Jr, R. P., 1982. Handbook on atmospheric diffusion (No. DOE/TIC-11223). National Oceanic and Atmospheric Administration, Oak Ridge, TN (USA).
- 645 Atmospheric Turbulence and Diffusion Lab.
- Hirst, B., Randell, D., Jones, M., Jonathan, P., King, B. and Dean, M., 2017. A new technique for monitoring the atmosphere above onshore carbon storage projects that can estimate the locations and mass emission rates of detected sources. *Energy Procedia*, 114, pp.3716-3728.
- Hmiel, B., Petrenko, V.V., Dyonisius, M.N., Buizert, C., Smith, A.M., Place, P.F., Harth, C., Beaudette, R., Hua, Q., Yang, B. and Vimont, I., 2020. Preindustrial 14 CH 4 indicates greater anthropogenic fossil CH<sub>4</sub> emissions. *Nature*, 578(7795), pp.409-412.
- 650 Höglund-Isaksson, L., 2017. Bottom-up simulations of methane and ethane emissions from global oil and gas systems 1980 to 2012. *Environmental Research Letters*, 12(2), p.024007.
- Humphries, R., Jenkins, C., Leuning, R., Zegelin, S., Griffith, D., Caldow, C., Berko, H. and Feitz, A., 2012. Atmospheric tomography: a Bayesian inversion technique for determining the rate and location of fugitive emissions. *Environmental science & technology*, 46(3), pp.1739-1746.
- 655 Jenkins, C., Kuske, T. and Zegelin, S., 2016. Simple and effective atmospheric monitoring for CO<sub>2</sub> leakage. *International Journal of Greenhouse Gas Control*, 46, pp.158-174.
- Joffre, S. M., and Laurila, T., 1988. Standard deviations of wind speed and direction from observations over a smooth surface. *Journal of Applied Meteorology*, 27(5), 550-561.
- 660 Konschnik, K. and Jordaan, S.M., 2018. Reducing fugitive methane emissions from the North American oil and gas sector: a proposed science-policy framework. *Climate Policy*, 18(9), pp.1133-1151.
- Kuske, T., Jenkins, C., Zegelin, S., Mollah, M. and Feitz, A., 2013. Atmospheric tomography as a tool for quantification of CO<sub>2</sub> emissions from potential surface leaks: Signal processing workflow for a low accuracy sensor array. *Energy Procedia*, 37, pp.4065-4076.
- 665 Lewicki, J.L. and Hilley, G.E., 2009. Eddy covariance mapping and quantification of surface CO<sub>2</sub> leakage fluxes. *Geophysical Research Letters*, 36(21).



- Loh, Z., Leuning, R., Zegelin, S., Etheridge, D., Bai, M., Naylor, T. and Griffith, D., 2009. Testing Lagrangian atmospheric dispersion modelling to monitor CO<sub>2</sub> and CH<sub>4</sub> leakage from geosequestration. Atmospheric Environment, 43(16), pp.2602-2611.
- Luhar, A.K., Etheridge, D.M., Leuning, R., Loh, Z.M., Jenkins, C.R. and Yee, E., 2014. Locating and quantifying greenhouse gas emissions at a geological CO<sub>2</sub> storage site using atmospheric modeling and measurements. Journal of Geophysical Research: Atmospheres, 119(18), pp.10-959.
- Mønster, J.G., Samuelsson, J., Kjeldsen, P., Rella, C.W. and Scheutz, C., 2014. Quantifying methane emission from fugitive sources by combining tracer release and downwind measurements—a sensitivity analysis based on multiple field surveys. Waste Management, 34(8), pp.1416-1428.
- Omara, M., Sullivan, M.R., Li, X., Subramanian, R., Robinson, A.L. and Presto, A.A., 2016. Methane emissions from conventional and unconventional natural gas production sites in the Marcellus Shale Basin. Environmental science & technology, 50(4), pp.2099-2107.
- Omara, M., Zimmerman, N., Sullivan, M.R., Li, X., Ellis, A., Cesa, R., Subramanian, R., Presto, A.A. and Robinson, A.L., 2018. Methane emissions from natural gas production sites in the United States: Data synthesis and national estimate. Environmental science & technology, 52(21), pp.12915-12925.
- Peischl, J., Ryerson, T.B., Brioude, J., Aikin, K.C., Andrews, A.E., Atlas, E., Blake, D., Daube, B.C., De Gouw, J.A., Dlugokencky, E. and Frost, G.J., 2013. Quantifying sources of methane using light alkanes in the Los Angeles basin, California. Journal of Geophysical Research: Atmospheres, 118(10), pp.4974-4990.
- Pétron, G., Karion, A., Sweeney, C., Miller, B.R., Montzka, S.A., Frost, G.J., Trainer, M., Tans, P., Andrews, A., Kofler, J. and Helmig, D., 2014. A new look at methane and nonmethane hydrocarbon emissions from oil and natural gas operations in the Colorado Denver-Julesburg Basin. Journal of Geophysical Research: Atmospheres, 119(11), pp.6836-6852.
- Qian, W. and Venkatram, A., 2011. Performance of steady-state dispersion models under low wind-speed conditions. Boundary-layer meteorology, 138(3), pp.475-491.
- Ravikumar, A.P. and Brandt, A.R., 2017. Designing better methane mitigation policies: the challenge of distributed small sources in the natural gas sector. Environmental Research Letters, 12(4), p.044023.
- Ro, K.S., Johnson, M.H., Hunt, P.G. and Flesch, T.K., 2011. Measuring trace gas emission from multi-distributed sources using vertical radial plume mapping (VRPM) and backward Lagrangian stochastic (bLS) techniques. Atmosphere, 2(3), pp.553-566.
- Saunio, M., Stavert, A.R., Poulter, B., Bousquet, P., Canadell, J.G., Jackson, R.B., Raymond, P.A., Dlugokencky, E.J., et al., 2019. The global methane budget 2000-2017. Earth Syst. Sci. Data Discuss., <https://doi.org/10.5194/essd-2019-128>.



- Tominaga, Y. and Stathopoulos, T., 2013. CFD simulation of near-field pollutant dispersion in the urban environment: A review of current modeling techniques. *Atmospheric Environment*, 79, pp.716-730.
- U.S. EPA, 2014: Other Test Method (OTM) 33 and 33A Geospatial Measurement of Air Pollution-Remote Emissions Quantification-Direct Assessment (GMAP-REQ-DA), available at:  
705 <https://www.epa.gov/emc/emc-other-test-methods>.
- van Leeuwen, C., Hensen, A. and Meijer, H.A., 2013. Leak detection of CO<sub>2</sub> pipelines with simple atmospheric CO<sub>2</sub> sensors for carbon capture and storage. *International Journal of Greenhouse Gas Control*, 19, pp.420-431.
- Vaughn, TL, Bell, CS, Yacovitch, TI, Roscioli, JR, Herndon, SC, Conley, S, Schwietzke, S, Heath, GA,  
710 Pétron, G and Zimmerle, D 2017 Comparing facility-level methane emission rate estimates at natural gas gathering and boosting stations. *Elem Sci Anth*, 5: 71. DOI: <https://doi.org/10.1525/elementa.257>.
- Wilson, R. B., Start, G. E., Dickson C. R. and Ricks, N. R.: Diffusion under Low Wind speed Conditions near Oak Ridge, TN. NOAA Tech. Memo. ERL ARL-61, Idaho Falls, Idaho (1976).
- Yacovitch, T.I., Daube, C. and Herndon, S.C., 2020. Methane emissions from offshore oil and gas  
715 platforms in the Gulf of Mexico. *Environmental Science & Technology*, 54(6), pp.3530-3538.
- Yacovitch, T.I., Neiningen, B., Herndon, S.C., van der Gon, H.D., Jonkers, S., Hulskotte, J., Roscioli, J.R. and Zavala-Araiza, D., 2018. Methane emissions in the Netherlands: The Groningen field. *Elem Sci Anth*, 6(1).
- Yver Kwok, C., Laurent, O., Guemri, A., Philippon, C., Wastine, B., Rella, C. W., Vuillemin, C., Truong,  
720 F., Delmotte, M., Kazan, V., Darding, M., Lebègue, B., Kaiser, C., Xueref-Rémy, I., and Ramonet, M.: Comprehensive laboratory and field testing of cavity ring-down spectroscopy analyzers measuring H<sub>2</sub>O, CO<sub>2</sub>, CH<sub>4</sub> and CO, *Atmos. Meas. Tech.*, 8, 3867–3892.
- Zavala-Araiza, D., Alvarez, R.A., Lyon, D.R., Allen, D.T., Marchese, A.J., Zimmerle, D.J. and Hamburg, S.P., 2017. Super-emitters in natural gas infrastructure are caused by abnormal process conditions. *Nature communications*, 8(1), pp.1-10.  
725
- Zavala-Araiza, D., Lyon, D., Alvarez, R.A., Palacios, V., Harriss, R., Lan, X., Talbot, R. and Hamburg, S.P., 2015. Toward a functional definition of methane super-emitters: Application to natural gas production sites. *Environmental science & technology*, 49(13), pp.8167-8174.